Atmospheric Research 214 (2018) 296–310

Contents lists available at ScienceDirect

Atmospheric Research

journal homepage: www.elsevier.com/locate/atmosres

Responses of the hydrological regime to variations in meteorological factors under climate change of the Tibetan plateau

Ruida Zhong, Yanhu He, Xiaohong Chen*

Center for Water Resources and Environment Research, Sun Yat-sen University, Guangzhou 510275, China

ARTICLE INFO

Keywords:
Climate change
Meteorological factor
Response of hydrology
GCM
Tibetan plateau
Lancang River basin

ABSTRACT

Meteorological factors and the hydrologic cycle of the Tibetan plateau (TP) significantly influence the water resource supply, ecology, and social economy of wide downstream areas in Asia. This study evaluates changes in meteorological factors (e.g., precipitation, air temperature, and snowfall) and corresponding responses in the hydrological regime under future climate change scenarios in both the TP and the downstream areas. The Lancang River basin (LRB), located in the southeast TP and known as the upper Mekong River basin, is selected as the case study area. Future climate change projections are derived from five independent GCMs of CMIP5 and their multi-model ensemble. The variable infiltration capacity (VIC) distributed hydrological model is used to generate streamflow projections in future scenarios. Results show that precipitation and air temperature in both the lower LRB (representing the downstream area of TP) and upper LRB (representing the area in TP) are expected to increase substantially in the future, with higher increments in air temperature found in the upper LRB under high-emission scenarios. Snowfall, snow water equivalent (SWE), and snowmelt are commonly found to decrease with increasing air temperature, and the snow melt time tends to be earlier. Significantly increasing mean and extreme streamflow caused by increasing precipitation are anticipated in the future. The low flow shows much higher relative increments at the upstream of TP, which is mainly caused by changes in snow regulating (decreased snowfall and earlier snowmelt). However, those effects show weak influence on the streamflow in the downstream area, which would be more largely impact by the local precipitation change. In the future, irrigation, hydropower, and navigation in the TP could benefit from increased low flow in the TP, but the consistently increasing extreme high flow may indicate greater flood risk in the TP and downstream areas.

1. Introduction

High mountains and plateau areas are sources of most great rivers worldwide, collectively named the “water tower of the world” (Viviroli et al., 2007). These areas are important for the fresh water supply, ecological balance, and social economy of downstream areas (He et al., 2014; Huss et al., 2008; Immerzeel et al., 2016; Lutz et al., 2016). The Tibetan plateau (TP), known as the “water tower of Asia,” is the source of several main rivers in Asia including the Yangtze, Yellow, Mekong, Ganges, and Brahmaputra Rivers. The TP provides fresh water to an area spanning approximately 5.6 million km^2 and over 1.4 billion populations (Immerzeel et al., 2010).

Under the impact of global climate change and increasing greenhouse gas (GHG) emissions over the past decades, the global air temperature is expected to increase continuously, and the global pattern of precipitation is also expected to change throughout the 21st century (IPCC, 2007; IPCC, 2013). As a result, meteorological factors, hydrological cycle and ecology in many regions worldwide have evolved or are expected to change significantly in the future (Allen and Ingram, 2002; Wang et al., 2015, 2017b, 2018; Winsemius et al., 2015; Wu et al., 2017, 2018). The hydrological cycle of high mountain and plateau areas, especially the TP, are sensitive to climate change associated with global warming. That is because these areas are typically covered by vast snow, glacier, permafrost, and seasonally frozen soil, all of which can regulate the streamflow by temporarily restoring the water in solid form, and alsoserved as important resources for the streamflow supplied for the local and downstream areas (Bhatti et al., 2016; Cuo et al., 2014; Kraaijenbrink et al., 2017; Lutz et al., 2014; Pervez and Henebry, 2015; Shen et al., 2018).

Increased air temperature and a decrease in snow content in the TP have been observed in many studies, and some researchers have also found that these changes could alter runoff discharge, redistribute streamflow, and contribute to overall ecosystem change in the TP (Bibi et al., 2018; Gao et al., 2016; Immerzeel et al., 2013; Jain et al., 2010;

* Corresponding author.
E-mail address: eescxh@mail.sysu.edu.cn (X. Chen).

https://doi.org/10.1016/j.atmosres.2018.08.008
Received 26 April 2018; Received in revised form 18 July 2018; Accepted 16 August 2018
Available online 18 August 2018
0169-8095/

Lamsal et al., 2017; Tahir et al., 2011). Climate-change-induced cryospheric and hydrological alterations in the TP could not only impact the local environment, but also directly affect the ecological environment and human society that located in the downstream area (Cuo et al., 2014). Therefore, it is necessary to further evaluate changes in meteorological factors and the hydrological response of both the TP and the downstream areas for future climate change scenarios.

The general circulation model (GCM) is regarded as the most feasible and effective tool for predicting future climate change (IPCC, 2013; Su et al., 2016; Zhang et al., 2016; Wang et al., 2017d). GCMs are physics-based models that simulate the global climate and are typically forcing by the GHG emission levels under different pre-established emission scenarios (Moss et al., 2010; Singh and Goyal, 2016; Tan et al., 2017). The latest Coupled Model Intercomparison Project Phase 5 (CMIP5) released over 50 GCM projections from 24 institutes around the world (Taylor et al., 2011), providing useful information for studies of future climate change. Some studies have been performed to evaluate and predict meteorological and hydrological change in high mountain and plateau areas based on GCM projections. Significantly decreasing ice volume in the TP under future scenarios has been identified in several studies, with increasing air temperature as the major driver (Immerzeel et al., 2010; Ji and Kang, 2013; Lutz et al., 2013). Alone with the change of cryospheric component and precipitation, the general increment of streamflow has been predicted in some basins in the TP, including Brahmaputra, the upper Indus and the upper Yellow basin (Li et al., 2013; Zhang et al., 2015; Lutz et al., 2016). Jain et al. (2010) found that increased air temperature would change the intra-annual distribution of the streamflow in the TP. Lutz et al. (2014) and Immerzeel et al. (2013) predicted that increased glacier melting would contribute to the increment of future streamflow in the TP, and increased precipitation would also be a main factor. However, due to the limited in-situ meteorological and hydrological observations in TP, existing studies on responses to climate change for TP are mostly based on the indirect retrieval data but based less on the local observations, and the hydrological models they used also usually lack in-situ calibration and validation for the TP, hence, they tend to focus on qualitative changes in meteorology and hydrology. Therefore, we suggest that the validation based on more in-situ meteorological and in-situ-calibrated hydrological model, and the further quantitative and detailed evaluation would be need. Moreover, the present studies are mostly focus on meteorological hydrological change for only the plateau areas, while influences on the downstream areas of TP where would be directly impact by the plateau area, are also less concerned.

The Lancang River basin (LRB) is located in the southeast area of the TP in southwest China (Fig. 1). The LRB is a typical plateau basin in TP thus could be a suitable case study for the meteorological and hydrological changes associated with climate change in the TP. The LRB is also known as the source region of the Mekong River, the largest river in southeast Asia, which passes through China, Burma, Laos, Thailand, Cambodia, and Vietnam. As one of the most important hydropower base, the LRB also provides abundant fresh water and hydropower resources for China (Fan et al., 2015) and exerts a notable impact on the rest of the Mekong River basin (Räsänen et al., 2017). Several studies have examined changes in the meteorological and hydrological regime of the Mekong River basin under climate change, exploring issues such as flood risk and hydrological extremes (Hoang et al., 2016; Wang et al., 2017b), and uncertainty of flow projections (Thompson et al., 2013). However, those studies mainly focused on the middle and lower Mekong, while the upper Mekong river basin located in the TP, i.e., the LRB, is still less concerned.

Above all, this study aims to further evaluate changes in meteorological factors (e.g., precipitation, snowfall, and air temperature) and corresponding responses in the hydrological regime (e.g., changes in runoff discharge and hydrological extremes) in the TP and the downstream areas under future climate change scenarios, taking the LRB as a representative case. Compared with former studies of the TP, we quantitatively predict and evaluate variations and trends in the meteorological factors, evaluate and compare the responses in mean and extreme streamflow for both the TP and its downstream areas in future scenarios. The variable infiltration capacity (VIC) model, a water- and energy-balance-based distributed hydrological model, is adopted to generate land surface hydrological process projections of future scenarios coupled with CMIP5 projections. This study would help to understand how hydrological regime changes in future in the TP and the downstream area of TP under climate change, and provide reference for water resource and hydropower planning, and flood forecasting in these areas.

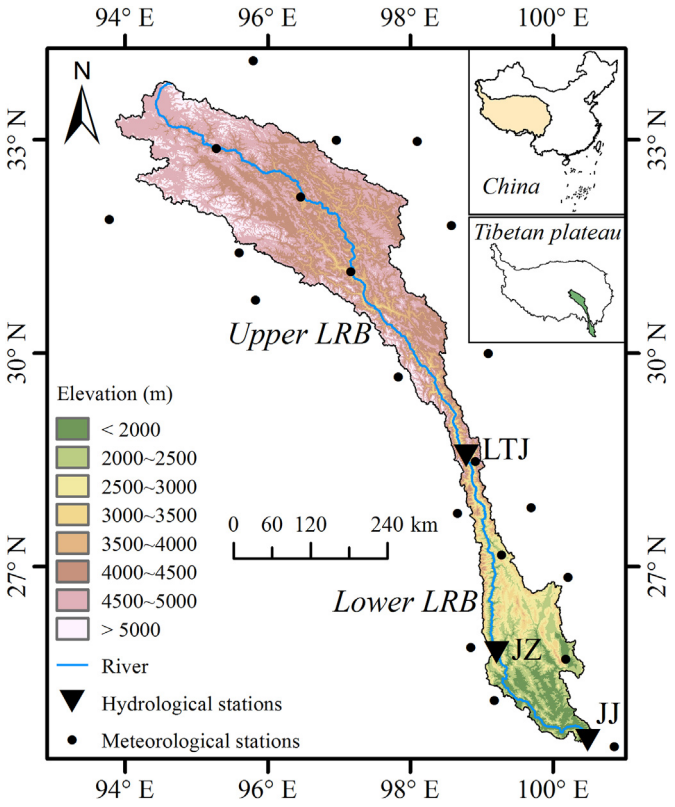

Fig. 1. Location and topography of the Lancang River basin (LRB).

2. Materials and methodology

2.1. Study area

The TP is located in the central Asia, southwest China with a mean elevation of above 4000 m, providing source water (consist of snow and glacial melt water, and liquid rainfall) for several main rivers of Asia. The Mekong River is one of the main river of Asia, and the LRB that located in southeast TP is the source region of the Mekong River. The LRB has a drainage area of approximately 108,766 km^2 controlled by the Jiajiu (JJ) hydrological station (see Fig. 1) and an annual mean streamflow of $3.96 \times 10^{10} m^3$ at the JJ station. The LRB can be divided into two parts, i.e. the upper LRB and lower LRB, according to distinctly different topography and climate characteristics by taking the Liutongjiang (LTJ) hydrological station as the boundary (Fig. 1). The upper LRB is located in the southeast of the TP with a mean elevation of 4500 m; it is dominated by an alpine and temperate plateau climate with mean annual precipitation of 572 mm and a mean air temperature of 2.6 °C. Vegetation is sparse in the upper LRB, which is mainly covered by glaciers, desert, tundra, and alpine grassland. The lower LRB is located in the west of the Yunnan-Guizhou plateau with a mean elevation of about 2500 m and a mainly sub-tropical monsoon climate

with annual mean precipitation of 1046 mm and a mean temperature of 14 °C. Landcover of the lower LRB largely consists of evergreen broadleaf forest, shrubs, and grassland. Precipitation in the LRB is abundant but temporally unevenly distributed, with nearly 90% of precipitation falling in the flood season (April to September). At present, most of the installed main hydropower plants are located in the lower LRB. The environment of the LRB is fragile and sensitive to climate change. Under the impact of climate change and human activities throughout previous decades, the hydrological cycle and distribution of water resources in the LRB have been altered (Räsänen et al., 2017; Zhao et al., 2012).

2.2. VIC hydrological model

The VIC hydrological model (Liang et al., 1994; Liang et al., 1996) is a macroscale grid-based distributed land surface process scheme. The VIC model can simulate the hydrometeorological process that occurs at the land surface–atmosphere interface based on water balance and energy balance, considering several factors (e.g., landcover, vegetation root zones, and soil heterogeneity). The VIC model can also simulate the freezing and thawing processes of snow, glaciers, and frozen soil based on water and energy budget (Cherkauer and Lettenmaier, 1999; Cherkauer and Lettenmaier, 2003) coupled with evapotranspiration, infiltration, and the runoff yield process. Therefore, VIC is a suitable approach for use in alpine and plateau basins such as the TP. The VIC model has also been successfully applied in plateau basins in several relevant studies (Meng et al., 2016; Tong et al., 2014; Wang et al., 2017c; Zhang et al., 2013).

Several topographical and physical parameters are necessary to run the VIC model. In this study, elevation data were obtained from the Shuttle Radar Topography Mission (SRTM) high-resolution digital elevation dataset (Hennig et al., 2001). Soil property parameters were collected from the Harmonized World Soil Database (HWSD) global soil classification and texture dataset (FAO, 2009) provided by the Food and Agriculture Organization. The landcover parameters were derived from the China land use remote sensing monitoring database based on the Landsat TM data (www.resdc.cn) (Liu et al., 2005). The VIC model was run at 0.25° spatial resolution to reproduce the land surface and streamflow process combined with GCM climate projections. The river network information for streamflow generation was obtained from the gridded global river network dataset provided by Wu et al. (2011, 2012).

Some parameters of the VIC model are difficult to determine and thus require calibration, such as the index of the variable infiltration capacity curve, baseflow generation parameters, and soil layer depth. Similar to the method in Xie et al. (2007), we calibrated the VIC model by adjusting each parameter individually because the model has relatively fewer parameters and usually requires a large computation time. The Pearson correlation coefficient (CC), Nash–Sutcliffe coefficient of efficiency (NSCE), log-NSCE, and relative bias (RB) are adopted to evaluate the simulation performance of the model, in which NSCE, log-NSCE and RB are regarded as the optimal functions for the model calibration. These performance indices are calculated as follows:

$$CC = \frac{\sum_{i=1}^{n}(S_i - \overline{S})(O_i - \overline{O})}{\sqrt{\sum_{i=1}^{n}(S_i - \overline{S})^2}\cdot\sqrt{\sum_{i=1}^{n}(O_i - \overline{O})^2}} \quad (1)$$

$$NSCE = 1 - \frac{\sum_{i=1}^{n}(S_i - O_i)^2}{\sum_{i=1}^{n}(O_i - \overline{O})^2} \quad (2)$$

$$log - NSCE = 1 - \frac{\sum_{i=1}^{n}(log(S_i) - log(O_i))^2}{\sum_{i=1}^{n}(log(O_i) - \overline{log(O_i)})^2} \quad (3)$$

$$RB = \left(\frac{\overline{S}}{\overline{O}} - 1\right) \times 100\% \quad (4)$$

where S_i and O_i are the simulated and observed series, and $\overline{S}$ and $\overline{O}$ are their respective mean values. The CC, NSCE, and log-NSCE describe the agreement between observed and simulated series, in which the log-NSCE is more sensitive to low values and the RB describes the systematic error between simulations and observations.

2.3. Historical observations

Meteorological observations of the historical period (1960–2016) were used to downscale the GCM projections and calibrate the VIC model. Precipitation data were obtained from the China Gauge-based Daily Precipitation Analysis (CGDPA) dataset (Shen and Xiong, 2015) provided by the China Meteorological Administration (CMA). The CGDPA is a daily gridded dataset with a spatial resolution of 0.25°, generated from precipitation records of over 2400 gauge stations in China using a climatology-based optimal interpolation (OI) method and therefore has high quality and accuracy (Shen and Xiong, 2015). Other meteorological data (e.g., air temperature, wind speed, sunshine duration, air pressure, and relative humidity) were derived from 22 meteorological stations located in or around the LRB (see Fig. 1). As the meteorological stations are sparsely distributed, meteorological data were interpolated into each 0.25° grid cell using the co-Kriging method based on elevation. Shortwave radiation data are calculated from the sunshine duration using the Angstrom formula (Martinez-Lozano et al., 1985).

Daily streamflow observations from three hydrological stations located from the upper to lower LRB (i.e., the Liutongjiang (LTJ), Jiuzhou (JZ), and Jiajiu (JJ) station) were used to calibrate the VIC model and validate streamflow simulation performance. To evaluate the snow simulation performance of the VIC model, a long-term snow depth retrieval product of China based on passive microwave (PMW) remote sensing (hereafter referred to as SDPMW) (Che et al., 2008; Dai et al., 2015) was used to validate snow depth simulation. The SDPMW is generated from passive microwave data using an improved Chang's algorithm corrected by the in-situ snow depth observations in China (Che et al., 2008; Dai et al., 2015); thus, it is highly accurate and reliable in China and is suitable for validating snow simulation results in this study.

2.4. CMIP5 projections

Five GCM of CMIP5 were selected to explore future climate change: CanESM2, CNRM-CM5, IPSL-CM5A-LR, MIROC-ESM, and MPI-ESM-LR

Table 1
Summary of the selected GCMs.

GCM	Institution	Resolution
CanESM2	Canadian Centre for Climate Modelling and Analysis, Canada	128 × 64
CNRM-CM5	Centre National de Recherches Météorologiques, France	256 × 128
IPSL-CM5A-LR	Institute Pierre-Simon Laplace, France	96 × 96
MIROC-ESM	Atmosphere and Ocean Research Institute (The University of Tokyo), National Institute for Environmental Studies, and Japan Agency for Marine-Earth Science and Technology, Japan	128 × 64
MPI-ESM-LR	Max Planck Institute for Meteorology, Germany	192 × 96

(see Table 1). To ensure reliability and representativeness of future climate projections, GCMs were selected from different branches of the GCM family tree provided by Knutti et al. (2013) and are therefore relatively independent in future climate projections. Simulation performance and data availability were also considered in GCM selection. The CNRM-CM5 and IPSL-CM5A-LR have been found to perform well on reproducing precipitation (Huang et al., 2013a; Su et al., 2013; Wang and Chen, 2013; Wang et al., 2017d) while CanESM2, CNRM-CM5, MPI-ESM-LR, and MIROC-ESM are found to perform well on air temperature simulation (Chen and Frauenfeld, 2014; Su et al., 2013; Wang and Chen, 2013; Wang et al., 2017d). To obtain a single, robust, and stable climate projection to represent several GCMs, the multi-model ensemble (MME) (Krishnamurti et al., 2000; Murphy et al., 2004) was also derived by taking the average of the GCM projections.

The GCMs usually run under different GHG emission scenarios for a future period. The representative concentration pathways (RCPs) (Moss et al., 2010) are the emission scenarios adopted in the CMIP5 and IPCC AR5. The RCP2.6, RCP4.5, and RCP8.5 scenarios were selected for future climate projections in this study, in which RCP2.6 represents the lowest GHG emissions level and RCP8.5 represents the highest.

The daily GCM climate projection data for historical (1960–2005) and future scenarios (2006–2100) were derived from the Earth System Grid Federation (ESGF) website (esgf-data.dkrz.de). Meteorological variables of the GCMs used to force the VIC model include precipitation, near-surface air temperature, near-surface wind speed, incoming shortwave radiation, and relative humidity. Because the spatial resolution of the GCMs is usually coarse (typically > 100 km), a downscaling procedure is necessary to generate a finer GCM projection so as to meet the demands of regional studies (Wang and Chen, 2013). The bias-corrected climate imprint (*BCCI*) statistical downscaling method (Hunter and Meentemeyer, 2005; Werner and Cannon, 2016) was adopted to downscale the GCM projections due to satisfactory performance and lower computational demand (Dibike et al., 2018; Werner and Cannon, 2016).

3. Model calibration and validation

3.1. Calibration and validation of the VIC model

The VIC model was first calibrated to carry out land surface process and streamflow simulations. The model parameters of VIC for the entire LRB were calibrated with streamflow observations at the JJ station for 1960–1980. The rest of streamflow observations at the JJ station (1981–2006) were used to validate the calibration results, and those at the LTJ (1987–2006) and JZ (1967–2006) stations were used to evaluate the streamflow simulation performance of the VIC model in the upstream of the LRB. Results (see Fig. 2) show that the VIC model generally performs satisfactorily at the three stations. VIC performance at the JJ station is acceptable with an NSCE of approximately 0.7 and RB of about 8% for both the calibration and validation periods. The log-NSCE, over 0.8, is also relatively high. For the LTJ and JZ stations, the VIC model performs better, with a high NSCE and log-NSCE of nearly 0.8 and a low RB below 5%, suggesting that the calibrated VIC model is reliable and reasonable for simulating the streamflow of the LRB.

Fig. 3 shows time series data for the SDPMW-retrieved and VIC-simulated snow depth. Generally, snow cover duration and annual snow depth trends are reasonably reproduced by the VIC model, although some large deviations appear in simulated snow depth magnitude. According to Fig. 4, the VIC model could reproduce the spatial pattern of the snow depth by comparing them to the SDPMW retrievals, although some discrepancies exist. Because of the sparsely-distributed meteorological stations and the complex terrain throughout the LRB, meteorological data might not always accurately reveal the local climate characteristics of the LRB even though the co-Kriging interpolation method was adopted, resulting in apparent deviations between the SDPMW and VIC snow depth. Measurement errors in the SDPMW data and simulation errors in the VIC model might also affect the evaluation results of snow depth simulation shown this study. In general, the snow depth simulation results from the VIC model are acceptable; hence, we suggest that the VIC model is reasonable for reproducing the land surface process of the LRB.

3.2. Validation of the GCM-based simulations

GCM projections for the historical period and future scenarios were downscaled based on local meteorological observations and then were used as inputs to run the VIC model. The annual mean of the downscaling results (precipitation and air temperature) and VIC simulation results (snowfall, snow water equivalent (SWE), snowmelt, and runoff) of the GCM projections during the historical period (1960–2005) for each month are shown in Fig. 5. Except for precipitation, air temperature, and runoff, “Observations” in Fig. 5 refer to the VIC simulations forced by the meteorological observations. Results of the upper and lower LRB were evaluated separately due to distinctly different climates representing different areas. Precipitation and air temperature for the GCM projections are close to the observations. As for snowfall, SWE, and snowmelt, relatively poor consistencies and higher uncertainties occur between the observations and GCM simulations, especially for SWE. High uncertainties of snow simulation coupled with GCMs have also appeared in relevant studies (Kudo et al., 2017); however, the GCMs still reproduced the seasonal pattern of snow cover. For the streamflow simulation, all GCMs reproduced the intra-annual variation of runoff and fit well with the low flow at the three hydrological stations, although the high flow from July to September was underestimated. Simulation results of the MME present the best fit with the observations, highlighting the superiority of the MME to any individual GCM and echoing results from Pierce et al. (2009). In general, the GCMs could reveal the climate and hydrological regime of the LRB and therefore are capable to evaluate the impact of climate change on the LRB in TP.

4. Results and analysis

4.1. Projection of meteorological factor change

We first evaluated changes in two basic meteorological factors: precipitation and air temperature. Trends in the annual precipitation and mean air temperature of the upper and lower LRB for future scenarios (2006–2100) were quantified using Sen's slope (Sen, 1968) and are listed in Table 2. The significance of the trends was derived by the Mann-Kendall (M-K) test (Kendall, 1975; Mann, 1945).

Precipitation in both the upper and lower LRB tend to increase significantly in future scenarios, among the five GCMs except little cases. As projected by MME, those trends are among 5 mm to 26 mm per decades for the three scenarios, and higher trends are found for the high-emission scenarios (e.g. RCP8.5). The upper LRB (representing the inner TP) shows lower absolute increasing trend of precipitation than lower LRB (representing the downstream areas), but their relative trends (quantified by relative Sen's slope) are closer, in which upper LRB is little higher. As for the significance of trend, upper LRB generally presents more significant in precipitation than lower LRB, with generally more GCMs show significance of 0.05 level in increasing precipitation trends for the three RCP scenarios. As for air temperature, similar to the former studies, almost all GCMs show significant increasing trends under the three scenarios, for both the upper and lower LRB. Upper LRB commonly shows higher increasing trends in air temperature than lower LRB under higher-emission scenarios, average of 0.31 °C and 0.71 °C per decade for RCP4.5 and RCP8.5 respectively.

Fig. 6 show changes in annual mean precipitation and air temperature for each month between the future scenarios and historical period for the upper and lower LRB. The future period is set to 2051–2100 because the emission levels of the three RCP scenarios show

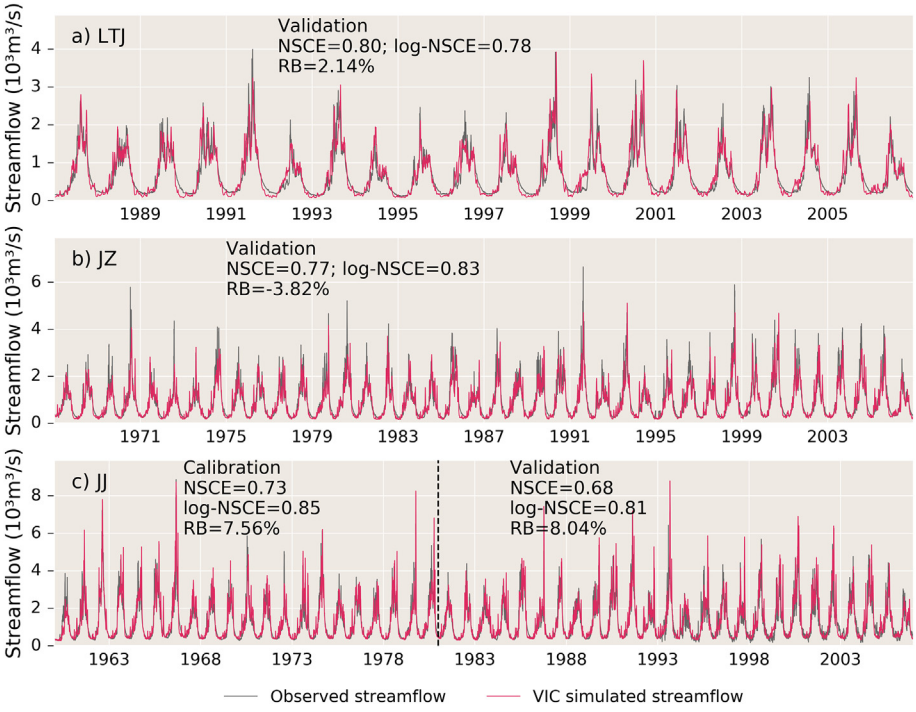

Fig. 2. Observed and simulated daily streamflow at the (a) Liutongjiang, (b) Jiuzhou, and (c) Jiajiu stations.

relatively less difference before the mid-21st century. Apparently, changes in precipitation and air temperature show similar intra-annual variations. Precipitation generally presents absolute and relative increment in spring and summer (April to July) but shows decrement in autumn (September to November) in both the upper and lower LRB. Although MME shows that the upper and lower LRB have similar magnitude of precipitation increment, MME for lower LRB might be largely impact by CanESM2 which shows much higher increment, hence we suggest that upper LRB should have higher precipitation increment than lower LRB. The change in air temperature presents similar seasonal patterns as precipitation under the three scenarios, with the highest increment in spring (March to May) and lowest increment in autumn (September to October), and the upper LRB presents higher increment in air temperature than the lower LRB. Can-ESM2 and IPSL-CM5A-LR present the highest magnitude of change in precipitation and air temperature, whereas MPI-ESM-LR and CNRM-CM5 generally demonstrate the smallest change.

Greatly increased air temperature in the TP should indicate significant changes in the snow process. Next, changes in snowfall, SWE and snowmelt would be evaluated in the upper LRB (entirely in the TP) for future scenarios. SWE, and snowmelt are considered meteorological factors because they potentially induce change in streamflow; the glacier is not considered because it contributes little to streamflow for the LRB (Lutz et al., 2014; Zhang et al., 2013). Table 3 shows that annual snowfall, mean SWE and snowmelt decrease significantly especially under high-emission scenarios (i.e., RCP4.5 and RCP8.5), as almost all GCMs indicate significant decreasing trends. As projected by MME, annual snowfall tends to decrease by 1.09 mm and 1.76 mm per decade under RCP4.5 and RCP8.5, respectively, implying that increased precipitation in the upper LRB cannot compensate for the loss of snowfall

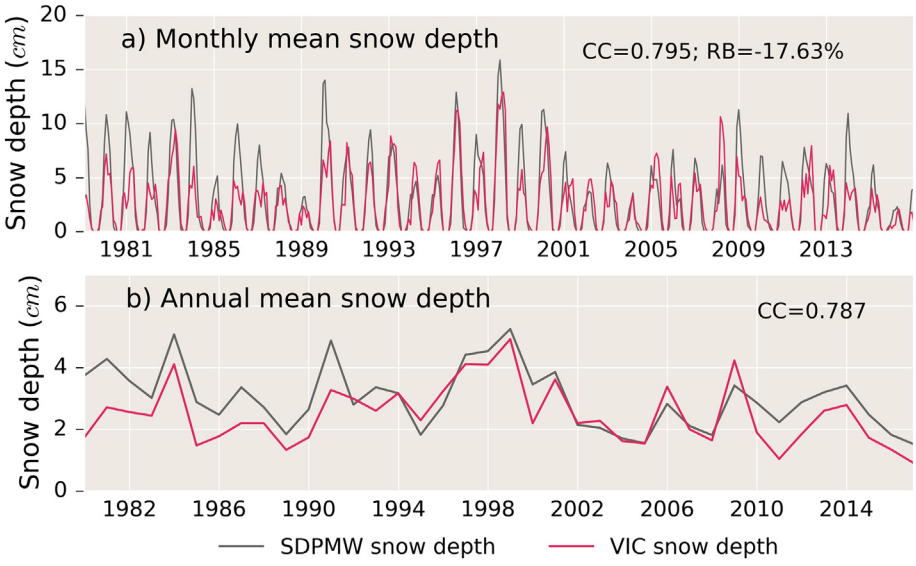

Fig. 3. SDPMW-retrieved and VIC-simulated (a) monthly and (b) annual areal average snow depth of the upper LRB.

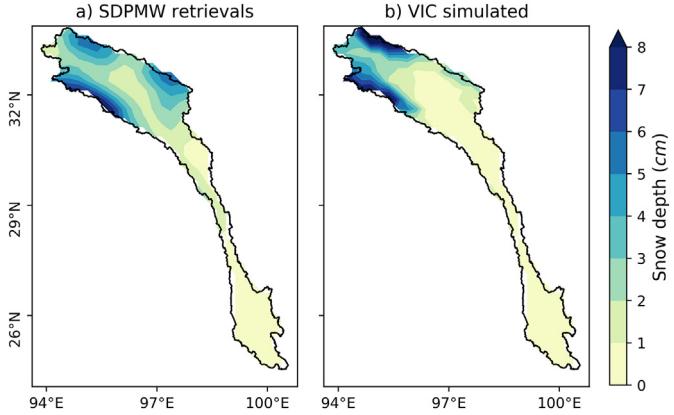

Fig. 4. Spatial distribution of the (a) SDPMW-retrieved and (b) VIC-simulated mean snow depth of the LRB.

resulting from increased air temperature. Correspondingly, the annual mean SWE and snowmelt averagely decrease by 0.24 mm and 1.12 mm per decade under RCP4.5, and 0.33 mm and 1.45 mm per decade under RCP8.5, respectively. CanESM2 presents the largest decrement of the snow component with a decreasing snowfall trend of −1.92 mm and −2.29 mm per decade under RCP4.5 and RCP8.5.

Fig. 7 shows seasonal changes in snow fall, SWE and snowmelt between the future scenarios (2051–2100) and historical period (1960–2005) in the upper LRB. The timeline of Fig. 7 begins with August. Larger decrements in snow are generally found under high-emission scenarios (e.g., RCP8.5), presumably due to increased air temperature. Snowfall is mostly lower in spring (February to May) and autumn (October and November), with less change in winter (November to January). Correspondingly, SWE shows the highest decrement in April to May, approximately 5.0 mm and 6.5 mm under RCP2.6 and RCP8.5, respectively. For January and February, changes of SWE are relatively less, perhaps due to less change in previous snowfall. Higher variation is found in SWE among the GCMs, but the trends are generally similar. Snowmelt tends to demonstrate less change in winter and early spring (November to April), although SWE decreases during the same time, but largely declines from May to June, which is similar to findings from Dibike et al. (2018); that is, the snow cover melting time becomes earlier, and less snow would therefore be available to melted in early summer.

4.2. Response in hydrological regime

We further evaluated changes in the hydrological regime of the TP for the future scenarios by taking the three stations (LTJ, JZ, and JJ) in the LRB as examples. The LTJ station is located in the plateau area and

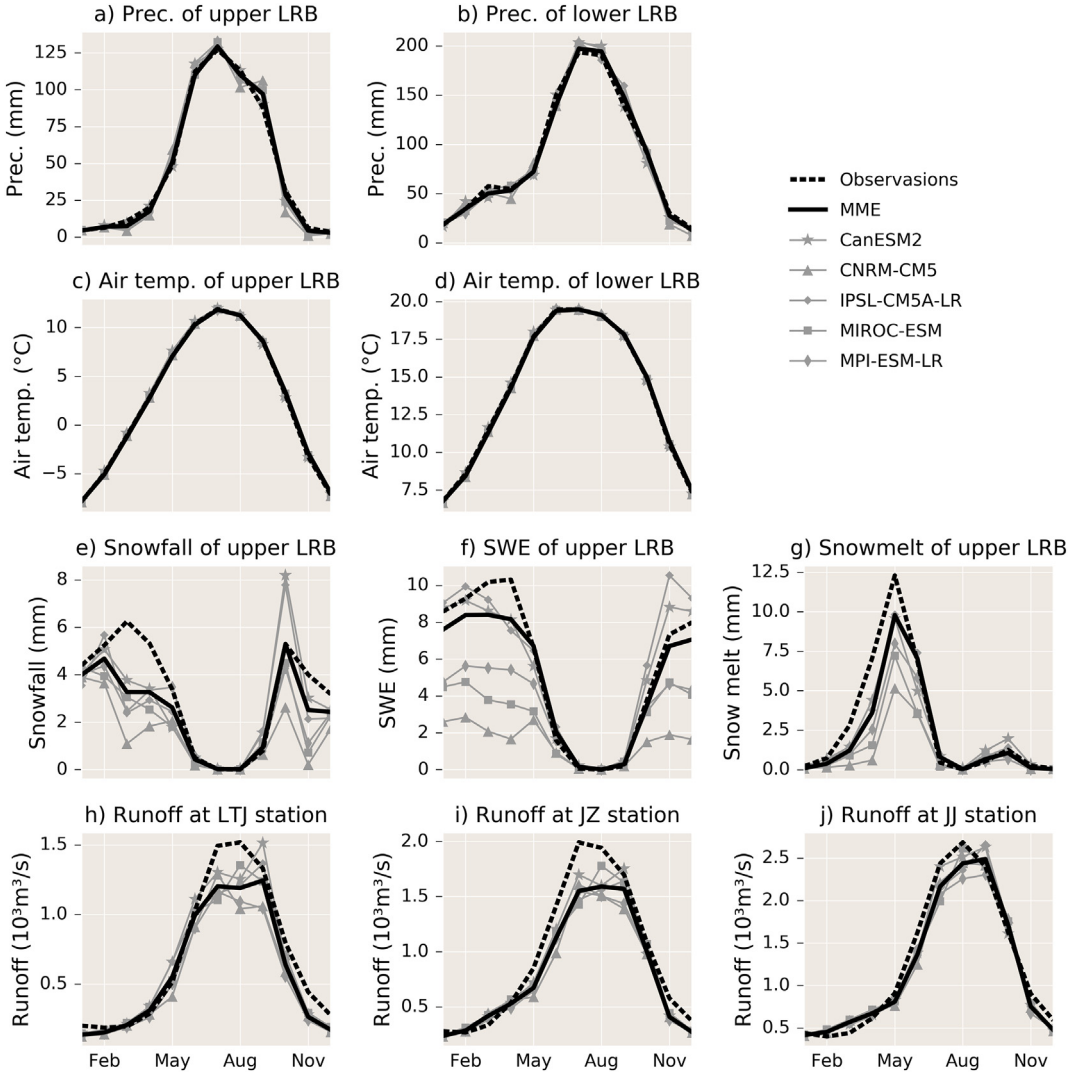

Fig. 5. Downscaling and simulation results of GCM projections during historical period (1960–2005).

Table 2
Sen's slope of annual precipitation and annual mean air temperature for future scenarios (2006–2100) in the upper and lower LRB. Note: values in brackets are percentages relative Sen's slope; asterisk indicates significance of trend at the 0.05 level based on the M-K test.

Scenarios	GCM	Annual precipitation (mm/10a (%/10a))		Air temperature (°C/10a)	
		Upper LRB	Lower LRB	Upper LRB	Lower LRB
RCP2.6	MME	5.09 (0.81%)*	5.94 (0.54%)	0.09*	0.08*
	CanESM2	6.50 (0.96%)*	30.87 (2.75%)*	0.05	0.08*
	CNRM-CM5	1.18 (0.19%)	5.10 (0.46%)	0.05*	0.09*
	IPSL-CM5A-LR	10.32 (1.63%)*	3.32 (0.32%)	0.11*	0.09*
	MIROC-ESM	6.49 (1.08%)*	2.14 (0.20%)	0.20*	0.13*
	MPI-ESM-LR	1.86 (0.34%)	−7.27 (−0.70%)	0.02	0.04*
RCP4.5	MME	11.56 (1.87%)*	15.97 (1.45%)*	0.31*	0.24*
	CanESM2	13.20 (1.96%)*	13.57 (1.09%)	0.33*	0.25*
	CNRM-CM5	5.49 (0.88%)	9.46 (0.88%)	0.21*	0.21*
	IPSL-CM5A-LR	16.28 (2.54%)*	7.99 (0.75%)	0.36*	0.30*
	MIROC-ESM	17.24 (2.90%)*	23.89 (2.25%)*	0.42*	0.23*
	MPI-ESM-LR	5.53 (0.98%)	17.39 (1.72%)*	0.25*	0.19*
RCP8.5	MME	21.09 (3.30%)*	26.06 (2.34%)*	0.71*	0.56*
	CanESM2	28.89 (4.24%)*	88.08 (7.65%)*	0.69*	0.56*
	CNRM-CM5	14.48 (2.26%)*	12.28 (1.04%)*	0.49*	0.40*
	IPSL-CM5A-LR	27.30 (4.05%)*	7.46 (0.72%)	0.85*	0.66*
	MIROC-ESM	26.23 (4.23%)*	21.50 (2.01%)*	0.90*	0.59*
	MPI-ESM-LR	6.27 (1.10%)*	0.90 (0.08%)	0.63*	0.57*

* The significance of the trend based on the Mann-Kendall trend test.

can directly reveal the hydrological regime of the TP. The lower stations (JZ and JJ) were also evaluated to assess the impact of the TP on the downstream areas. Mean runoff is used to represent runoff discharge, while the maximum 3-day (MX3D) runoff and minimum 7-day (MN7D) runoff (Lin et al., 2014; Richter et al., 1996; Smakhtin, 2001) are adopted as indices of extremely high and low flow, respectively. MX3D and MN7D are the maximum of the 3-day averaged and minimum of the 7-day averaged streamflow in a year respectively. Table 4 and Table 5 show the absolute and relative trends of the mean, MX3D, and MN7D runoff at the LTJ, JZ, and JJ stations, respectively.

Generally, the mean flow and extreme high and low flow at the three stations increase significantly for the future scenarios under RCP4.5 and RCP8.5. Trends with higher significance and higher absolute increment of streamflow are found for downstream stations (JZ and JJ) (Table 4), as their inherent streamflow are higher. While for the relative (percentage) increment of streamflow, especially for extreme low flow, higher relative recrements are found for the station closest to the TP (LTJ station), but, those increasing trends tend to become weaker as the distance to TP increases (Table 5). For instance, as projected by MME, MN7D runoff at the LTJ station (located in the TP) increases by 5.55% and 11.35% per decade under RCP4.5 and RCP8.5, respectively, nearly twice and four times those at the JZ and JJ stations

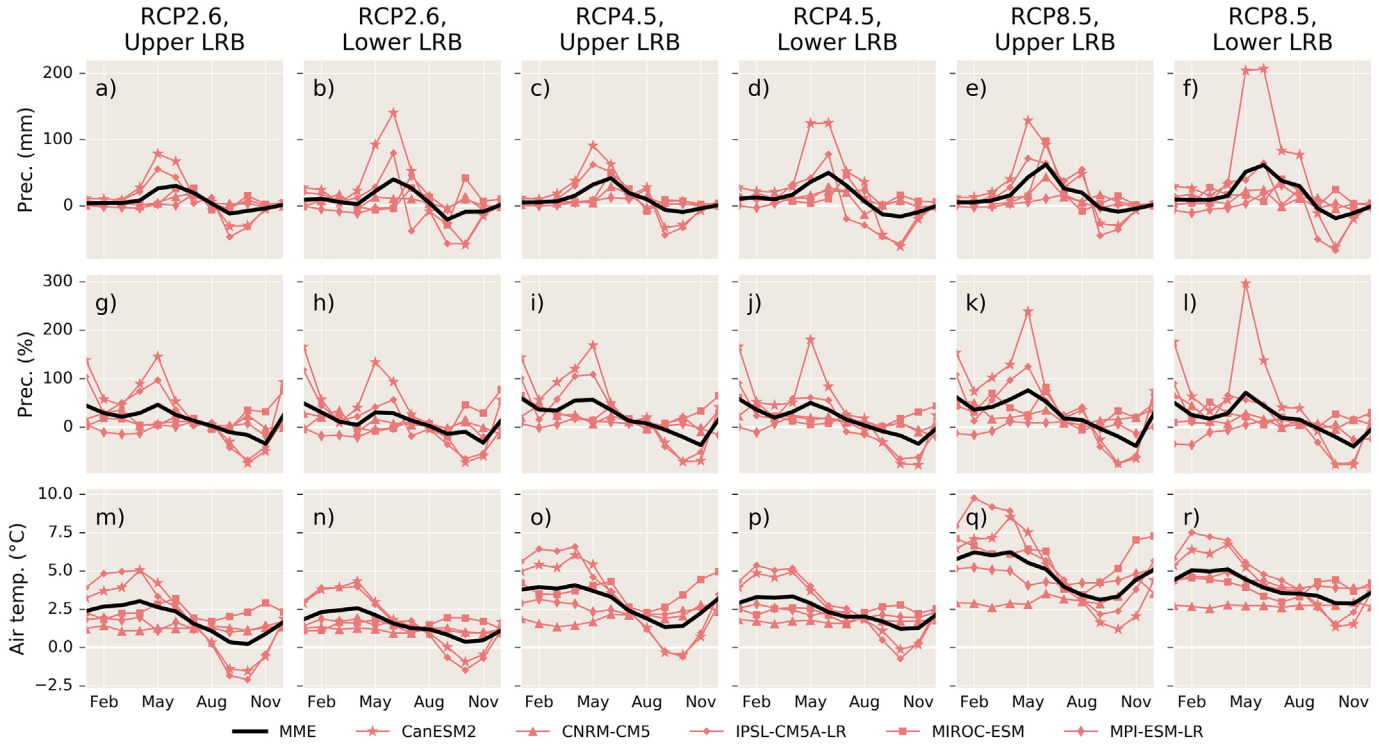

Fig. 6. Change in (a–l) precipitation and (m–r) air temperature, and (d–f) percentage relative change of precipitation between future scenarios (2051–2100) and historical period (1960–2005) for both the upper and lower LRB.

Table 3
Sen's slope of annual snowfall, mean SWE, and snowmelt for future scenarios (2006–2100) of the upper and lower LRB. Note: the asterisk indicates significance of trend at the 0.05 level based on the M-K test.

Scenarios	GCM	Snowfall (mm/10a)	SWE (mm/10a)	Snowmelt (mm/10a)
RCP2.6	MME	−0.19	−0.07*	−0.14
	CanESM2	0.30	0.12	1.24*
	CNRM-CM5	0.01	0.01	0.01
	IPSL-CM5A-LR	−0.53*	−0.13*	−0.62*
	MIROC-ESM	−0.55*	−0.06*	−0.44*
	MPI-ESM-LR	0.14	0.00	0.23
RCP4.5	MME	−1.09*	−0.24*	−1.12*
	CanESM2	−1.92*	−0.35*	−1.75*
	CNRM-CM5	−0.18	0.00	−0.12
	IPSL-CM5A-LR	−1.25*	−0.24*	−0.96*
	MIROC-ESM	−1.10*	−0.13*	−0.77*
	MPI-ESM-LR	−0.68*	−0.09*	−0.54*
RCP8.5	MME	−1.76*	−0.33*	−1.45*
	CanESM2	−2.29*	−0.47*	−1.36*
	CNRM-CM5	−0.73*	−0.06*	−0.76*
	IPSL-CM5A-LR	−1.94*	−0.24*	−1.21*
	MIROC-ESM	−1.84*	−0.12*	−0.81*
	MPI-ESM-LR	−1.18*	−0.09*	−0.64*

* The significance of the trend based on the Mann-Kendall trend test.

located downstream of the TP. Higher increment in low flow might be related to the early snowmelt in the upper LRB, and this impact of upper LRB on streamflow might be weaken as the distance to upper LRB increases. MX3D and mean runoff also show the highest relative change at the LTJ station (7.45% and 5.2% per decade, respectively, under RCP8.5), but differences with those of the JZ and JJ stations are smaller. Higher relative increment of precipitation in the plateau area than the downstream area shown in section 4.1 might be a main reason.

Among the scenarios, high-emission scenarios also show larger increment of streamflow, as MX3D runoff increases by among 194m^3/s to 374m^3/s per decade under RCP8.5, nearly 1.5 to 2.4 times that those under RCP4.5. MN7D runoff under RCP8.5 is also about twice of that those under RCP4.5.

Absolute and relative changes of the mean and extreme flow between the future scenarios (2051–2100) and historical period (1960–2005) are also evaluated (Figs. 8 and 9). Similar to the results above, JJ station presents the highest absolute increment in mean and MX3D runoff. For the relative change displayed in Fig. 9, the LTJ station (closest to TP), shows comparable increment for mean and MX3D runoff with JZ and JJ and much higher relative increment of MN7D runoff than JZ and JJ. Variations also exist among the GCMs, as CanESM2 and MIROC-ESM generally present the highest change in flow indices, but only MPI-ESM-LR shows little change and decrement while all the other GCMs shows similar increment patterns.

Changes in intra-annual variation of streamflow for the three hydrological stations in the future scenarios are further evaluated. The results are displayed in Figs. 10 and 11 for absolute and relative change, respectively. Although variations still exist among the GCMs, higher absolute increments are commonly found in flood season (May to August) but higher relative increments are generally found for low flow in dry season (November to April). These findings are corresponding to those of extreme high and low flow shown above. Among the three stations, higher relative increments for dry season are most significant for LTJ station that closest to TP (increases by about 50% to over 100% for dry season). However, those variation patterns apparently tend to diminished as the distance to TP increases. At JJ, the most downstream station, inter-annual variation of relative streamflow change is similar to changes in precipitation in lower LRB, and relative increment for dry season flow even lower than flood season.

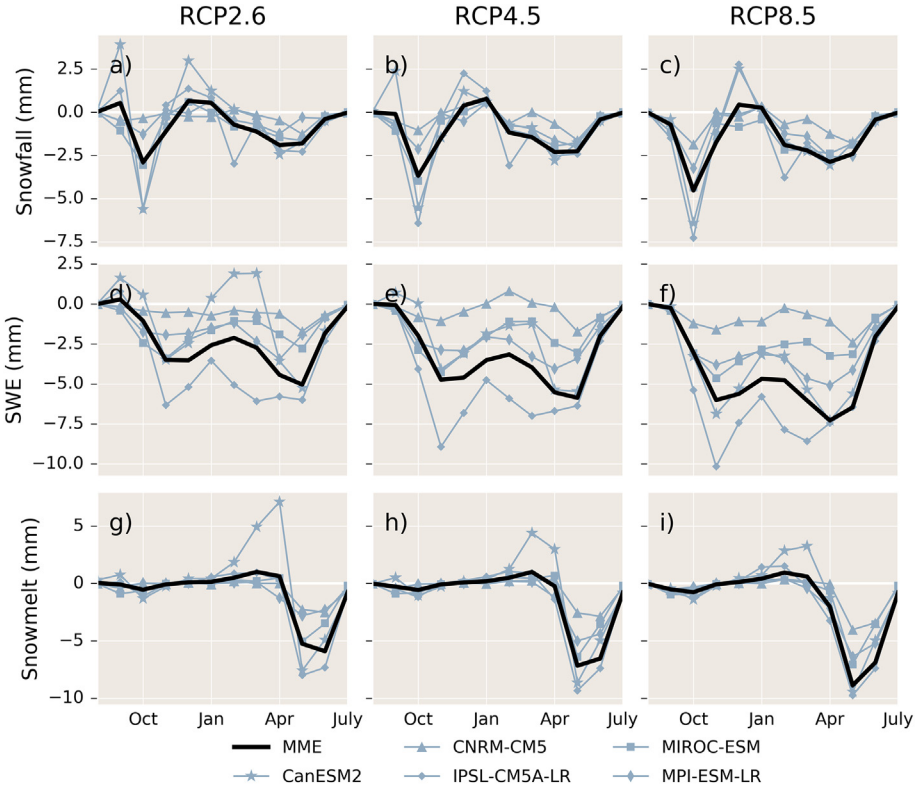

Fig. 7. Change in snowfall, SWE and snowmelt between the future scenarios (2051–2100) and historical period (1960–2005) in the upper LRB.

Table 4
Sen's slope of annual mean runoff, MX3D runoff, and MN7D runoff at the LTJ, JZ, and JJ stations for the future scenarios (2006–2100). Note: an asterisk indicates significance of trend at the 0.05 level based on the M-K test.

Scenarios	GCM	Mean runoff (m^3/s/10a)			MX3D runoff (m^3/s/10a)			MN7D runoff (m^3/s/10a)		
		LTJ	JZ	JJ	LTJ	JZ	JJ	LTJ	JZ	JJ
RCP2.6	MME	14.6*	16.6*	17.8*	61.4*	73.3*	87.0*	2.6*	2.8*	2.8*
	CanESM2	17.1*	30.8*	52.8*	69.2	174.7*	285.6*	3.3*	5.5*	6.8*
	CNRM-CM5	3.1	0.3	−0.1	−22.0	−51.1	16.9	1.7*	1.5	2.1
	IPSL-CM5A-LR	29.7*	32.5*	26.9*	185.9*	151.0*	73.7	1.9*	1.1	0.7
	MIROC-ESM	18.5*	18.6*	17.3	79.5	72.1	60.0	3.5*	4.6*	4.3*
	MPI-ESM-LR	10.4*	9.5	1.2	24.2	47.0	−43.1	2.6*	2.1	0.7
RCP4.5	MME	22.8*	28.0*	34.4*	132.1*	128.0*	154.9*	6.8*	6.5*	5.9*
	CanESM2	25.6*	32.1*	34.2*	102.8*	109.0	111.9	5.7*	5.6*	5.2*
	CNRM-CM5	6.9	7.7	9.1	12.8	1.6	16.2	3.5*	3.6*	2.4
	IPSL-CM5A-LR	27.1*	26.9*	27.1*	208.9*	185.5*	190.4*	5.2*	3.7*	0.4
	MIROC-ESM	43.8*	55.5*	68.3*	222.8*	225.8*	268.1*	13.3*	16.7*	17.2*
	MPI-ESM-LR	7.3	14.9*	23.2*	16.4	81.8*	195.9*	4.5*	4.2*	5.3*
RCP8.5	MME	32.9*	40.3*	53.3*	193.8*	234.5*	373.8*	14.1*	13.8*	12.0*
	CanESM2	44.7*	75.7*	134.2*	196.0*	440.8*	1041.5*	15.6*	17.5*	18.7*
	CNRM-CM5	14.1*	16.3*	22.2*	59.1	64.9	50.4	6.0*	6.2*	5.6*
	IPSL-CM5A-LR	34.5*	33.8*	37.5*	214.5*	212.1*	268.6*	10.6*	8.5*	6.1*
	MIROC-ESM	66.9*	77.2*	87.5*	384.0*	365.5*	383.0*	30.3*	30.6*	28.9*
	MPI-ESM-LR	−1.8	−3.9	−7.1	11.8	−8.1	−12.7	6.0*	4.2*	0.8

* The significance of the trend based on the Mann-Kendall trend test.

Table 5
Percentage relative Sen's slope of annual mean runoff, MX3D runoff, and MN7D runoff at the LTJ, JZ, and JJ stations for the future scenarios (2006–2100). Note: an asterisk indicates significance of trend at the 0.05 level based on the M-K test.

Scenarios	GCM	Mean streamflow (%/10a)			MX3D streamflow (%/10a)			MN7D streamflow (%/10a)		
		LTJ	JZ	JJ	LTJ	JZ	JJ	LTJ	JZ	JJ
RCP2.6	MME	2.23*	1.86*	1.33*	2.36*	2.11*	1.55*	2.33*	1.34*	0.76*
	CanESM2	2.34*	3.07*	3.54*	2.49	4.63*	4.94*	2.79*	2.58*	1.90*
	CNRM-CM5	0.58	0.03	−0.01	−1.02	−1.51	0.30	1.53*	0.70	0.55
	IPSL-CM5A-LR	4.44*	3.60*	2.11*	7.81*	4.98*	1.57	1.91*	0.60	0.20
	MIROC-ESM	2.75*	1.99*	1.34	3.22	2.02	1.15	3.27*	2.13*	1.09*
	MPI-ESM-LR	1.99*	1.25	0.10	1.37	1.72	−0.93	2.42*	1.02	0.18
RCP4.5	MME	3.49*	3.03*	2.63*	5.12*	3.69*	2.79*	5.55*	3.02*	1.57*
	CanESM2	3.53*	3.05*	2.16*	4.05*	2.81	1.62	4.35*	2.51*	1.37*
	CNRM-CM5	1.16	0.84	0.68	0.56	0.04	0.33	3.03*	1.64*	0.62
	IPSL-CM5A-LR	3.78*	2.98*	2.17*	7.56*	5.76*	4.01*	4.76*	1.84*	0.12
	MIROC-ESM	6.74*	5.98*	5.31*	8.71*	7.07*	5.91*	10.94*	7.09*	4.24*
	MPI-ESM-LR	1.58	2.12*	2.26*	0.97	3.21*	4.90*	4.11*	2.09*	1.52*
RCP8.5	MME	5.20*	4.60*	4.17*	7.45*	6.82*	6.95*	11.35*	6.33*	3.30*
	CanESM2	7.02*	8.15*	9.85*	8.38*	13.05*	18.77*	13.40*	8.35*	5.18*
	CNRM-CM5	2.36*	1.77*	1.67*	2.57	1.89	0.87	4.71*	2.69*	1.42*
	IPSL-CM5A-LR	4.93*	3.81*	3.02*	8.63*	6.86*	5.75*	9.40*	4.27*	1.85*
	MIROC-ESM	10.41*	8.32*	6.70*	15.82*	10.28*	7.59*	22.78*	12.72*	7.11*
	MPI-ESM-LR	−0.45	−0.62	−0.74	0.81	−0.31	−0.32	5.81*	2.21*	0.23

* The significance of the trend based on the Mann-Kendall trend test.

5. Discussion

5.1. Change in meteorological factors and impact on hydrological regime

Some studies have explored the precipitation, air temperature, and snow cover change throughout the entire TP. Increment of air temperature and decrement of snow content have been observed and projected (Ji and Kang, 2013; Kraaijenbrink et al., 2017; Lutz et al., 2014; Wang et al., 2008). Commonly increasing precipitation has also been found in other basins in the TP, e.g. the upper Yellow and Brahmaputra River basins, although different GCMs were used in those studies (Li et al., 2013; Zhang et al., 2015). Though quantitative trend analysis and seasonal variations were not considered in the former studies, similar conclusions were drawn, suggesting the reliability of our results regarding projected meteorological factor change and representativeness for the entire TP.

In this study, we identified a generally increasing trend in streamflow and higher relative increment of low flow during the dry season (November to March), the magnitude of which tends to become more significant in the TP. This hydrological regime change could result from several evolving meteorological factors mentioned earlier (e.g., increased precipitation, decreased snowfall and snowmelt, and shift in snow melting time). A similar experiment was carried out by Lutz et al. (2014), who also found increased streamflow in the upper Salween and upper Mekong River basin (i.e., the upper LRB) and proposed increased precipitation as the dominant factor. They also suggested that a change in the proportion of snow and liquid water and shifting snow melting time might cause increased flow during the dry season and decreased flow during the flood season. However, further quantitative evaluation and comparison of variations in the hydrological regime and the relative analysis for the downstream areas were not considered, perhaps due to the different concentrations and lack of local observed information for the LRB. To obtain a more concrete and detailed projection of the hydrological regime change of the TP and the downstream

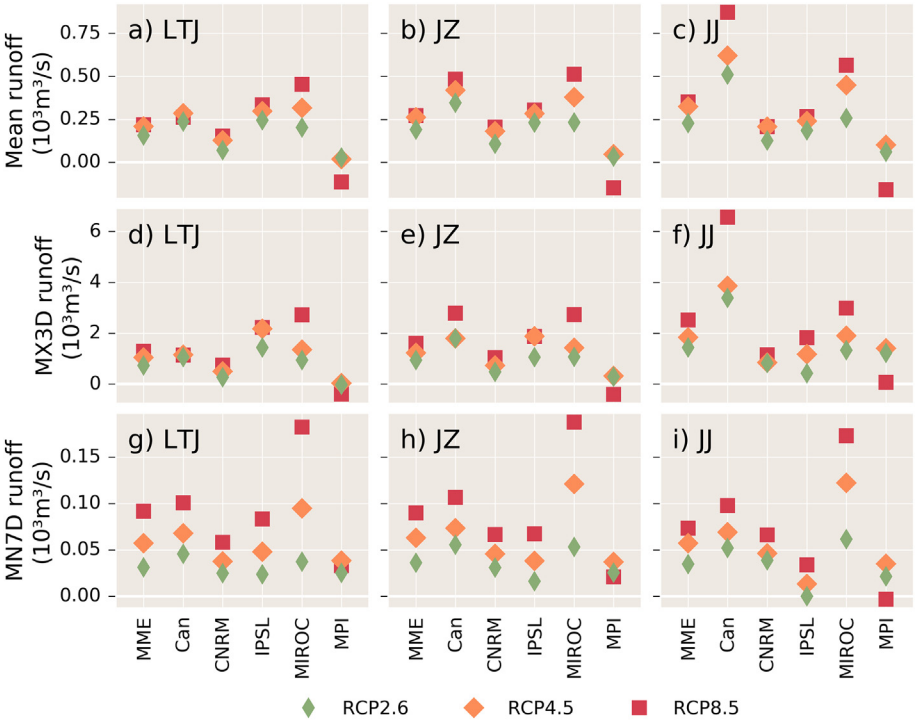

Fig. 8. Change of annual mean runoff, MX3D runoff, and MN7D runoff between the future scenarios (2051–2100) and historical period (1960–2005) at the (a, d, g) LTJ, (b, e, h) JZ, and (c, f, i) JJ stations.

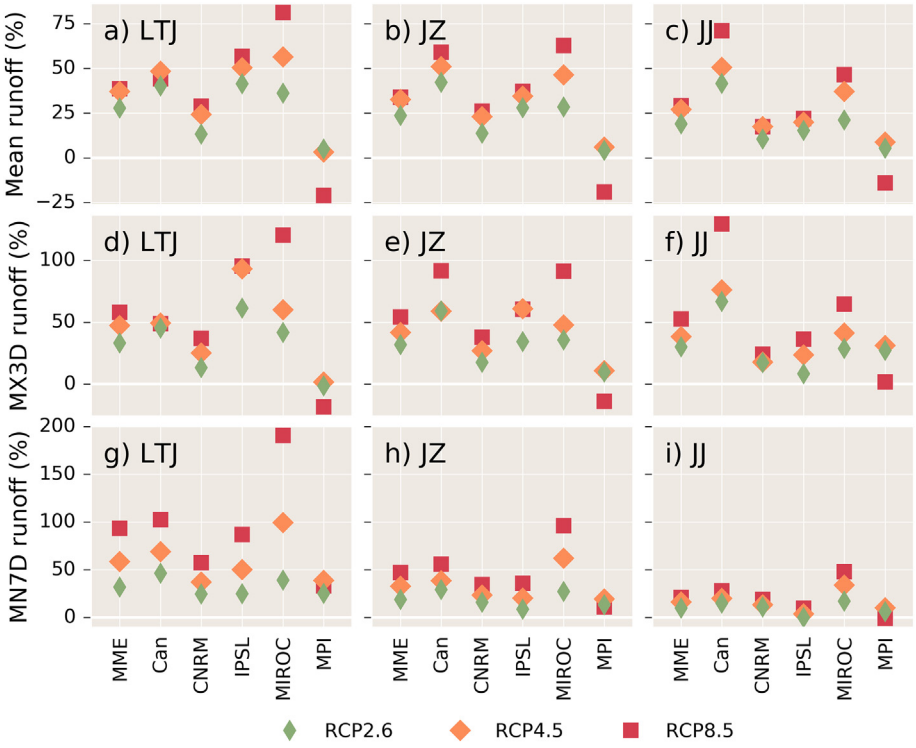

Fig. 9. Percentage relative change of annual mean runoff, MX3D runoff, and MN7D runoff between the future scenarios (2051–2100) and historical period (1960–2005) at the (a, d, g) LTJ, (b, e, h) JZ, and (c, f, i) JJ stations.

areas, compared with former studies, we further quantitatively performed and evaluated trends and variations of the runoff discharge and extreme low and high flow in the TP in future scenarios by taking the LRB as an example.

To determine how changes in the meteorological factor might influence changes in high and low flow, Fig. 12 visually depicts the relationship between changes in precipitation, snowfall, snowmelt, and streamflow in the upper LRB for the historical and future periods, using MME results as the example. The streamflow at the LTJ station is selected as an example because it is located in the TP and is thus affected directly by changes in snow in the TP. Differences in the amount of precipitation and snowfall tend become larger, particularly in spring

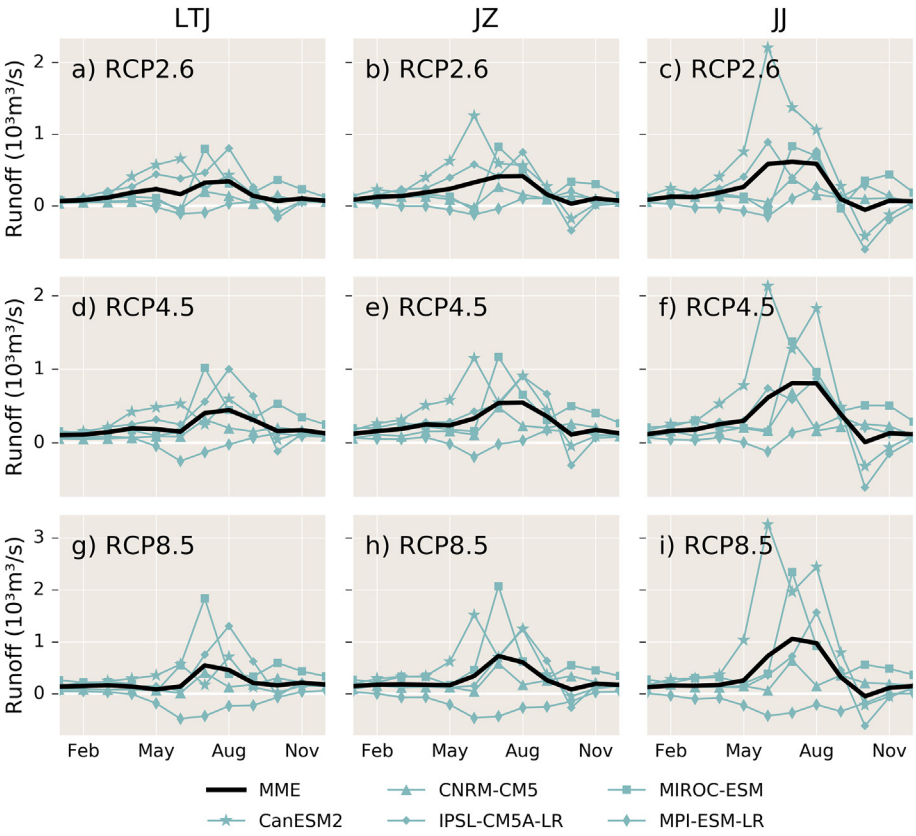

Fig. 10. Change in annual mean runoff for each month between the future scenarios (2051–2100) and historical period (1960–2005) of the (a, d, g) LTJ, (b, e, h) JZ, and (c, f, i) JJ stations.

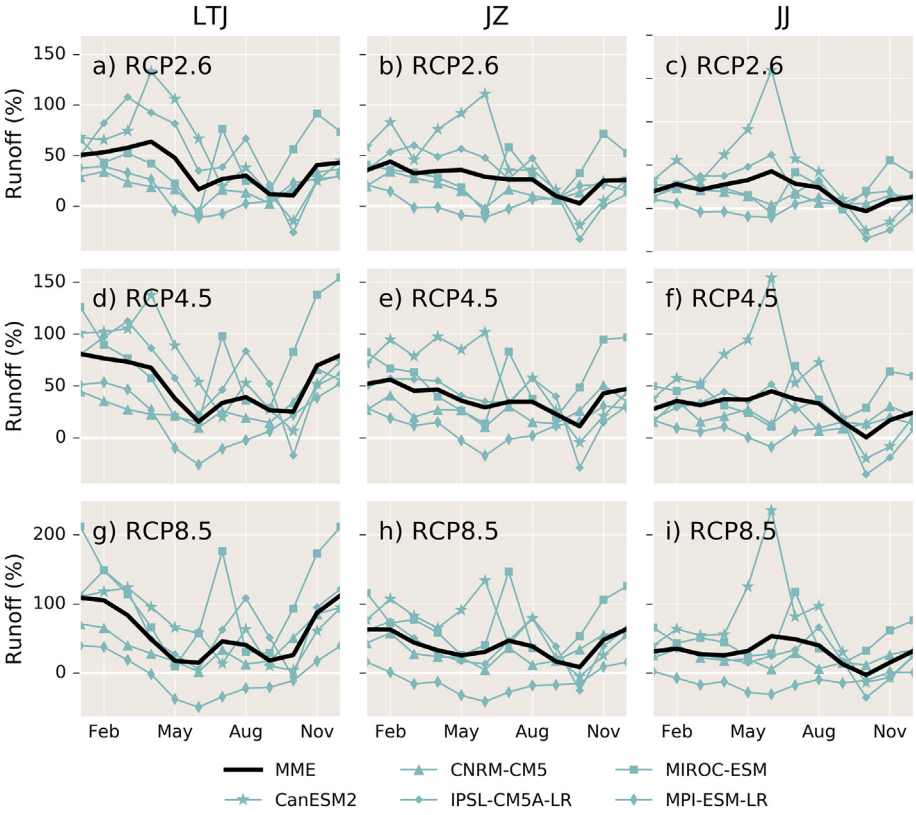

Fig. 11. Percentage relative change in annual mean runoff for each month between the future scenarios (2051–2100) and historical period (1960–2005) of the (a, d, g) LTJ, (b, e, h) JZ, and (c, f, i) JJ stations.

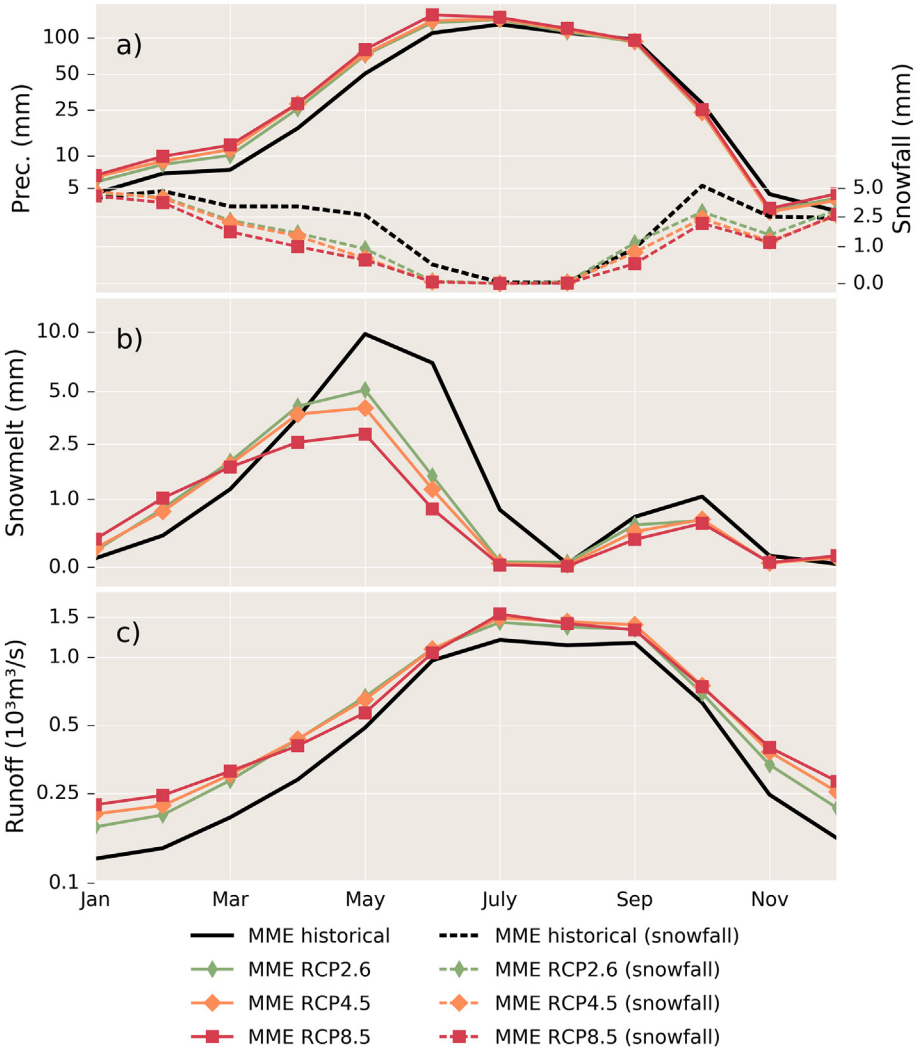

Fig. 12. Comparison of the MME-projected seasonal precipitation and (a) snowfall and (b) snowmelt in the upper LRB and (c) runoff at the LTJ station for the historical period and future scenarios.

(March to May) and October, indicating an increase of liquid water in the TP (Fig. 12a). Fig. 12b shows decreasing snowmelt and earlier snow melt time, as discussed in Section 3.2. The peak of snowmelt appears to shift from May and June to April to May, and the total amount of snowmelt is reduced by approximately 50–75%. As a result, snowmelt is maintained and increases slightly before April but declines sharply after May. Because the solid precipitation (in the form of snow and glaciers) could be stored for a relatively longer time than liquid precipitation (Lutz et al., 2014), an increase in the proportion of liquid precipitation and earlier melt time of snow would indicate a shift in the streamflow to the earlier months. Therefore, due to increased liquid precipitation resulting from lower snowfall in October and November and maintenance of the snowmelt water supply in December to April, runoff of the upper LRB shows large relative increment up to 100% while precipitation only increases up to 60% during the same period. Given decreased snowmelt after May, runoff shows the smallest increase in June, as increased precipitation compensates for the loss of snowmelt water. In all, the generally increased streamflow for the upper LRB mainly results from increasing precipitation, whereas intra-annual redistribution of streamflow result from decreased snowfall and earlier snow melt time owing to higher air temperature. This finding is consistent with that of Lutz et al. (2014) although different GCMs were used, suggesting the reasonability in our projected change in runoff discharge and hydrological extremes is.

For the lower stations (JZ and JJ), according to results in section 4.2, the pattern of intra-annual change in streamflow shown at the LTJ tend to diminished along with the distance to the TP. Although lower LRB has an area little than upper LRB, but the precipitation is much higher (Fig. 5a, b), and has almost no solid precipitation for the high air temperature. As a result, snow regulating effect (temporarily restoring water in solid form) in streamflow in upper LRB would be dilute by the inflow of lower LRB. In March and April, precipitation for lower LRB generally shows lower relative change (Fig.6) than the neighboring months, but relative streamflow increments of JZ and JJ are apparently higher than precipitation, indicating that contributions of the earlier-snowmelt-induced increased streamflow are also could be found for the downstream stations. However, for other months, especially for autumn (September to November), increased liquid precipitation in upper LRB has little compensation to the downstream streamflow, changes in streamflow for the lower stations are more consistent with those of precipitation of lower LRB. Therefore, changes in snow regulating of upper LRB might impact less on the downstream streamflow, as precipitation of the lower LRB is the main source for the downstream streamflow. Hence, for those areas more concentrations might should be paid for the precipitation of the downstream areas.

To further explore the meteorological change of the TP, spatial patterns of precipitation and air temperature change for flood season (May to September) and winter (December to February) around TP of

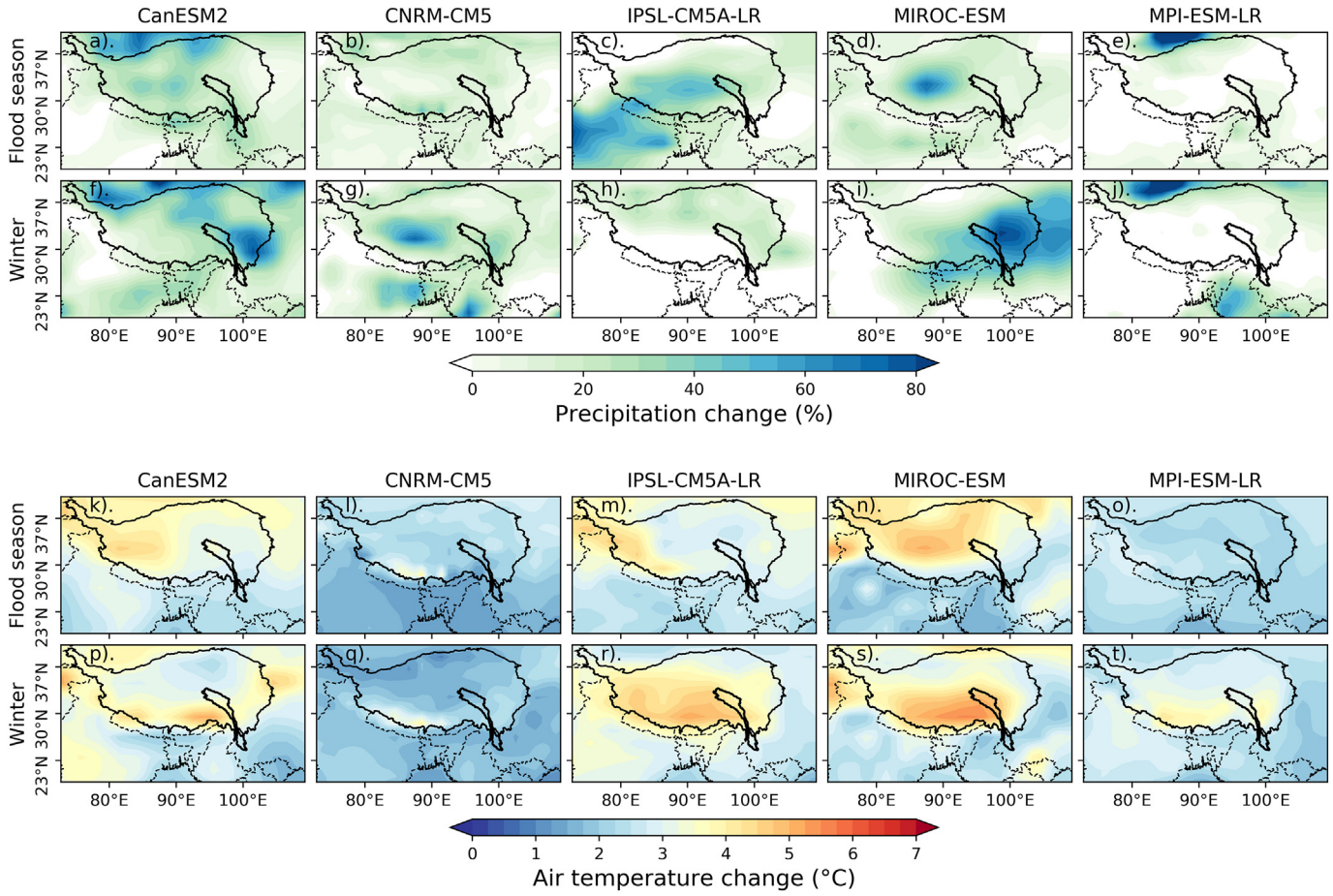

Fig. 13. Changes of precipitation (a–j) and air temperature (k–t) for flood season (May to September) and winter (December to February) around TP between 2051 and 2100 and 1960–2005 projected by the five GCMs under RCP4.5.

the five GCMs are analyzed and shown in Fig. 13. Those patterns are similar among the three RCP scenarios for all GCMs, hence only RCP4.5 with moderate GHG emission is selected as example. Spatial patterns of precipitation increment are quite different among the GCMs, but TP generally tends to present relative higher precipitation than the downstream areas like lower Yangtze, LRB, Brahmaputra, Ganges (Fig. 13a–j). Since precipitation in TP is mainly controlled by the south Asia, east Asia and Tibetan plateau summer monsoon in summer, and controlled by the winter westerlies in winter (Duan, 2013; Yang et al., 2014; Wang et al., 2016), global warming induced increasing air moisture and stronger monsoon (Hsu et al., 2012; Huang et al., 2013a, 2013b; Tan et al., 2018a, 2018b) might be the possible reason. Regional differences of air temperature increment between TP and downstream areas are more significant, as apparently higher increased air temperature is commonly found in winter among the GCMs, especially around Himalaya in south TP (Fig. 13p–t). This reveals that the other basins in TP would likely to facing the largely change in snow-regulated streamflow, similar to the results of this study. Although glacier water takes more part than snow in the streamflow in south and south west TP, the mechanism of how meteorologic change affect hydrology is expected to be similar. This also have been verified for the works applied in other parts of the TP, e.g. upper Indus, upper Yellow and Brahmaputra River basins (Jain et al., 2010; Lutz et al., 2014, 2016; Zhang et al., 2015). Hence, we expect similar increments in runoff discharge, high flow and low flows in those parts of TP. Increasing trends in the mean and low flow of the TP might indicate more abundant water resources for irrigation, navigation, and hydropower in downstream areas, while increment in extreme high-flow areas usually points to greater flood risk. However, since increasing low flow also results from changes in the cryosphere of the plateau area, this trend might also indicate a threat to the environment and ecology of the TP.

5.2. *Uncertainties among the GCM projections in VIC model simulation*

Uncertainties among GCM projections are typical in studies evaluating meteorological and hydrological shifts under climate change (Yuan et al., 2017). These uncertainties often result from different implementation and initiation of the GCMs. Using several independent GCMs and scenarios could clarify the uncertainties of future climate projections (Kudo et al., 2017; Yan et al., 2015). Variations between GCM projections also appear in our results, revealing some uncertainties. CanESM2, IPSL-CM5A-LR, and MIROC-ESM tend to present the most extreme projections for future changes in precipitation, air temperature, snow, and streamflow, while CNRM-CM5 and MPI-ESM-LR present conservative projections although GCMs were bias-corrected in the historical period. However, trends and intra-annual variations for changes in meteorological factors and streamflow were captured by over half the GCMs in most cases. For instance, relationships regarding the change of hydrological indices at different stations and scenarios are similar to MME in different GCMs, except MPI-ESM-LR (Figs. 8 and 10). The significant relative increment of low flow at LTJ is also shown by MPI-ESM-LR, although results are generally conservative (Fig. 11c).

MME is a recommended method because it can provide a robust and reliable comprehensive climate projection (Pierce et al., 2009; Wang et al., 2017a, 2017d); therefore, the method is adopted in this study by merging the five relative-independent GCMs. According to Pierce et al. (2009), skill of the GCMs tend to display an asymptote after including approximately five different GCMs. Although it is impossible to assess

climate projections for future periods, the MME simulations fit well with observations for the historical period (Fig. 5). Hence, we expect the MME to be stable and reasonable in providing future climate projections. Above all, the GCM projection and simulation results are acceptable for evaluating meteorological and hydrological regime changes in this study.

6. Conclusions

This study evaluates and predicts changes in meteorological factors and corresponding responses in the hydrology of the TP and its downstream area in future scenarios, using the LRB, a typical plateau basin, as a representative case. Future climate projections are based on five CMIP5 GCMs and their MME, and future land surface and streamflow process projections are simulated by the VIC model. Compared with previous studies, we further quantitatively evaluated trends and changes in intra-annual variation of the hydrological regime and extremes.

Results show that precipitation and air temperature are expected to increase significantly for the upper and lower LRB (representing the inner TP and downstream area of TP, respectively) in the future, with higher relative increments in air temperature in the upper LRB, especially under high emission scenarios. Changes in precipitation and air temperature in the future scenarios show apparent intra-annual variation. Precipitation mainly presents increment in April to July and little decrement in September and October, while air temperature presents higher increment in spring and less in autumn.

Substantially lower snowfall, SWE, snowmelt, and SIC are commonly found under RCP4.5 and RCP8.5 in the upper LRB (inner TP), and RCP8.5 shows larger decrement. Snowfall presents decrement in spring and winter but less change in winter. SWE demonstrates similar intra-annual patterns, whereas snowmelt shows decrement in May to June but little change in other months, indicating earlier snow melt.

Driven by the increasing precipitation, significantly increasing mean and extreme runoff are found in the LRB under future scenarios. And impacted by the decreased snowfall and earlier snowmelt, for the upstream station located in plateau area, extreme low flow is predicted for higher increment than extreme high flow, and higher relative increment is precited to occur in dry seasons (November to April), especially under high-emission scenarios. However, those effects of changes in snow to streamflow are weak for the downstream areas, as the change pattern that low flow increases more largely than high flow tends to diminished in the downstream area. Therefore, change in streamflow for the downstream area would be more largely impact by the local precipitation change.

Above all, mean, low and high streamflow are predicted to increase for TP, and upstream tends to presents higher increment in low flow. Higher discharge and low flow reflect more available resources for irrigation, navigation, and hydropower in the TP and downstream areas, whereas higher extreme high flow would indicate greater flood risk in the TP in the future.

Acknowledgements

The research is financially supported by the National Key R&D Program of China (2017YFC0405900) and National Natural Science Foundation of China (Grant Nos.: 91547202, 51479216 and 51509127).

References

Allen, M.R., Ingram, W.J., 2002. Constraints on future changes in climate and the hydrologic cycle. Nature 419 (6903), 224.
Bhatti, A.M., Koike, T., Shrestha, M., 2016. Climate change impact assessment on mountain snow hydrology by water and energy budget-based distributed hydrological model. J. Hydrol. 543, 523–541.
Bibi, S., Wang, L., Li, X., Zhou, J., Chen, D., Yao, T., 2018. Climatic and associated cryospheric, biospheric, and hydrological changes on the Tibetan Plateau: a review. Int. J. Climatol. 38, e1–e17.
Che, T., Xin, L., Jin, R., Armstrong, R., Zhang, T., 2008. Snow depth derived from passive microwave remote-sensing data in China. Ann. Glaciol. 49 (1), 145–154.
Chen, L., Frauenfeld, O.W., 2014. Surface air temperature changes over the twentieth and twenty-first centuries in China simulated by 20 CMIP5 models. J. Clim. 27 (11), 3920–3937.
Cherkauer, K.A., Lettenmaier, D.P., 1999. Hydrologic effects of frozen soils in the upper Mississippi River basin. J. Geophys. Res. Atmos. 104 (D16), 19599–19610.
Cherkauer, K.A., Lettenmaier, D.P., 2003. Simulation of spatial variability in snow and frozen soil. J. Geophys. Res. Atmos. 108 (D22).
Cuo, L., Zhang, Y., Zhu, F., Liang, L., 2014. Characteristics and changes of streamflow on the Tibetan Plateau: a review. J. Hydrol. 2, 49–68.
Dai, L., Che, T., Ding, Y., 2015. Inter-calibrating SMMR, SSM/I and SSMI/S Data to improve the consistency of snow-depth products in China. Remote Sens. Basel 7, 7212–7230.
Dibike, Y., Eum, H., Prowse, T., 2018. Modelling the Athabasca watershed snow response to a changing climate. J. Hydrol. 15, 134–148.
Duan, A., 2013. The Tibetan Plateau summer monsoon in the CMIP5 simulations. J. Clim. 26 (19), 7747–7766.
Fan, H., He, D., Wang, H., 2015. Environmental consequences of damming the mainstream Lancang-Mekong River: a review. Earth-Sci. Rev. 146, 77–91.
FAO, 2009. Harmonized World Soil Database Version 1.1.
Gao, Q., Guo, Y., Xu, H., Ganjurjav, H., Li, Y., Wan, Y., Qin, X., Ma, X., Liu, S., 2016. Climate change and its impacts on vegetation distribution and net primary productivity of the alpine ecosystem in the Qinghai-Tibetan Plateau. Sci. Total Environ. 554-555, 34–41.
He, Z.H., Parajka, J., Tian, F.Q., Blöschl, G., 2014. Estimating degree day factors from MODIS for snowmelt runoff modeling. Hydrol. Earth Syst. Sci. 11 (7), 4773–4789.
Hennig, T.A., Kretsch, J.L., Pessagno, C.J., Salamonowicz, P.H., Stein, W.L., 2001. The shuttle radar topography mission. Rev. Geophys. 1 (2), 361.
Hoang, L.P., Lauri, H., Kummu, M., Koponen, J., Van Vliet, M.T.H., Supit, I., Leemans, R., Kabat, P., Ludwig, F., 2016. Mekong River flow and hydrological extremes under climate change. Hydrol. Earth Syst. Sci. Discuss. 20 (7), 3027–3041.
Hsu, P., Li, T., Luo, J., Murakami, H., Kitoh, A., Zhao, M., 2012. Increase of global monsoon area and precipitation under global warming: a robust signal? Geophys. Res. Lett. 39 (6).
Huang, D.Q., Zhu, J., Zhang, Y.C., Huang, A.N., 2013a. Uncertainties on the simulated summer precipitation over Eastern China from the CMIP5 models. J. Geophys. Res. Atmos. 118 (16), 9035–9047.
Huang, P., Xie, S., Hu, K., Huang, G., Huang, R., 2013b. Patterns of the seasonal response of tropical rainfall to global warming. Nat. Geosci. 6, 357–361.
Hunter, R.D., Meentemeyer, R.K., 2005. Climatologically aided mapping of daily precipitation and temperature. J. Appl. Meteorol. 44 (10), 1501–1510.
Huss, M., Farinotti, D., Bauder, A., Funk, M., 2008. Modelling runoff from highly glacierized alpine drainage basins in a changing climate. Hydrol. Process. 22 (19), 3888–3902.
Immerzeel, W.W., Beek, L.P.H.V., Bierkens, M.F.P., 2010. Climate change will Affect the Asian water towers. Science 328 (5984), 1382.
Immerzeel, W.W., Pellicciotti, F., Bierkens, M.F.P., 2013. Rising river flows throughout the twenty-first century in two Himalayan glacierized watersheds. Nat. Geosci. 6, 742–745.
Immerzeel, W.W., Wanders, N., Lutz, A., Shea, J., Bierkens, M., 2016. Reconciling High-Altitude Precipitation in the Upper Indus Basin with Glacier Mass Balances and Runoff. EGU General Assembly Conference.
IPCC, 2007. The Physical Science Basis. Contribution of Working Group I to the Fourth Assessment Report of the Intergovernmental Panel on Climate Change. Cambridge University Press, Cambridge, United Kingdom, New York, USA.
IPCC, 2013. Climate Change 2013: The Physical Science Basis. Contribution of Working Group I to the Fifth Assessment Report of the Intergovernmental Panel on Climate Change. Cambridge University Press, Cambridge, United Kingdom, New York, USA.
Jain, S.K., Goswami, A., Saraf, A.K., 2010. Assessment of Snowmelt Runoff using remote sensing and effect of climate change on runoff. Water Resour. Manag. 24 (9), 1763–1777.
Ji, Z., Kang, S., 2013. Projection of snow cover changes over China under RCP scenarios. Clim. Dyn. 41 (3–4), 589–600.
Kendall, M., 1975. Multivariate Analysis. Griffin. pp. 123–131.
Knutti, R., Masson, D., Gettelman, A., 2013. Climate model genealogy: Generation CMIP5 and how we got there. Geophys. Res. Lett. 40 (6), 1194–1199.
Kraaijenbrink, P., Bierkens, M., Lutz, A.F., Immerzeel, W.W., 2017. Impact of a global temperature rise of 1.5 degrees Celsius on Asia's glaciers. Nature 549 (7671), 257–260.
Krishnamurti, T.N., Kishtawal, C.M., Zhang, Z., Larow, T., Bachiochi, D., Williford, E., Gadgil, S., Surendran, S., 2000. Multimodel ensemble forecasts for weather and seasonal climate. J. Clim. 13 (23), 4196–4216.
Kudo, R., Yoshida, T., Masumoto, T., 2017. Uncertainty analysis of impacts of climate change on snow processes: case study of interactions of GCM uncertainty and an impact model. J. Hydrol. 548.
Lamsal, P., Kumar, L., Shabani, F., Atreya, K., 2017. The greening of the Himalayas and Tibetan Plateau under climate change. Glob. Planet. Chang. 159, 77–92.
Liang, X., Lettenmaier, D.P., Wood, E.F., Burges, S.J., 1994. A simple hydrologically based model of land surface water and energy fluxes for general circulation models. J. Geophys. Res. Atmos. 99 (D7), 14415–14428.
Liang, X., Wood, E.F., Lettenmaier, D.P., 1996. Surface soil moisture parameterization of the VIC-2L model: evaluation and modification. Glob. Planet. Chang. 13 (1), 195–206.

Li, F., Zhang, Y., Xu, Z., Teng, J., Liu, C., Liu, W., Mpelasoka, F., 2013. The impact of climate change on runoff in the southeastern Tibetan Plateau. J. Hydrol. 505, 188–201.
Lin, K., Lv, F., Chen, L., Singh, V.P., Zhang, Q., Chen, X., 2014. Xinanjiang model combined with curve number to simulate the effect of land use change on environmental flow. J. Hydrol. 519, 3142–3152.
Liu, J., Liu, M., Tian, H., Zhuang, D., Zhang, Z., Zhang, W., Tang, X., Deng, X., 2005. Spatial and temporal patterns of China's cropland during 1990-2000: an analysis based on Landsat TM data. Remote Sens. Environ. 98 (4), 442–456.
Lutz, A.F., Immerzeel, W.W., Gobiet, A., Pellicciotti, F., Bierkens, M.F.P., 2013. Comparison of climate change signals in CMIP3 and CMIP5 multi-model ensembles and implications for Central Asian glaciers. Hydrol. Earth Syst. Sci. 17 (9), 3661–3677.
Lutz, A.F., Immerzeel, W.W., Shrestha, A.B., Bierkens, M.F.P., 2014. Consistent increase in high Asia's runoff due to increasing glacier melt and precipitation. Nat. Clim. Chang. 4 (7), 587–592.
Lutz, A.F., Immerzeel, W.W., Kraaijenbrink, P.D.A., Shrestha, A.B., Bierkens, M.F.P., 2016. Climate change impacts on the upper indus hydrology: sources, shifts and extremes. PLoS ONE 11 (11).
Mann, H.B., 1945. Nonparametric tests against trend. Econometrica 13 (3), 245–259.
Martinez-Lozano, J.A., Tena, F., Onrubia, J.E., Jdela, R., 1985. The historical evolution of the Angstrom formula and its modifications: review and bibliography. Agric. Forest Meteorol. 33 (2), 109–128.
Meng, F., Su, F., Yang, D., Tong, K., Hao, Z., 2016. Impacts of recent climate change on the hydrology in the source region of the Yellow River basin. J. Hydrol. 6 (C), 66–81.
Moss, R.H., Edmonds, J.A., Hibbard, K.A., Manning, M.R., Rose, S.K., Vuuren, D.P.V., Carter, T.R., Emori, S., Kainuma, M., Kram, T., 2010. The next generation of scenarios for climate change research and assessment. Nature 463 (7282), 747–756.
Murphy, J.M., Sexton, D.M.H., Barnett, D.N., Jones, G.S., Webb, M.J., Collins, M., Stainforth, D.A., 2004. Quantification of modelling uncertainties in a large ensemble of climate change simulations. Nature 430 (7001), 768–772.
Pervez, M.S., Henebry, G.M., 2015. Assessing the impacts of climate and land use and land cover change on the freshwater availability in the Brahmaputra River basin. J. Hydrol. 3, 285–311.
Pierce, D.W., Barnett, T.P., Santer, B.D., Gleckler, P.J., 2009. Selecting global climate models for regional climate change studies. P. Natl. Acad. Sci. USA 106 (21), 8441–8446.
Räsänen, T.A., Someth, P., Lauri, H., Koponen, J., Sarkkula, J., Kummu, M., 2017. Observed river discharge changes due to hydropower operations in the Upper Mekong Basin. J. Hydrol. 545, 28–41.
Richter, B.D., Baumgartner, J.V., Powell, J., Braun, D.P., 1996. A method for assessing hydrologic alteration within ecosystems Un Métro para Evaluar Alteraciones Hidrológicas dentro de Ecosistemas. Conserv. Biol. 10 (4), 1163–1174.
Sen, P.K., 1968. Estimates of the regression coefficient based on Kendall's Tau. J. Am. Stat. Assoc. 63 (324), 1379–1389.
Shen, Y., Xiong, A., 2015. Validation and comparison of a new gauge-based precipitation analysis over mainland China. Int. J. Climatol. 36 (1), 252–265.
Shen, Y., Shen, Y., Fink, M., Kralisch, S., Chen, Y., Brenning, A., 2018. Trends and variability in streamflow and snowmelt runoff timing in the southern Tianshan Mountains. J. Hydrol. 557, 173–181.
Singh, V., Goyal, M.K., 2016. Analysis and trends of precipitation lapse rate and extreme indices over North Sikkim eastern Himalayas under CMIP5ESM-2M RCPs experiments. Atmos. Res. 167, 34–60.
Smakhtin, V.U., 2001. Low flow hydrology: a review. J. Hydrol. 240 (3), 147–186.
Su, F., Duan, X., Chen, D., Hao, Z., Cuo, L., 2013. Evaluation of the global climate models in the CMIP5 over the Tibetan Plateau. J. Clim. 26 (10), 3187–3208.
Su, B., Huang, J., Gemmer, M., Jian, D., Tao, H., Jiang, T., Zhao, C., 2016. Statistical downscaling of CMIP5 multi-model ensemble for projected changes of climate in the Indus River Basin. Atmos. Res. 178-179, 138–149.
Tahir, A.A., Chevallier, P., Arnaud, Y., Neppel, L., Ahmad, B., 2011. Modeling snowmelt-runoff under climate scenarios in the Hunza River basin, Karakoram Range, Northern Pakistan. J. Hydrol. 409 (1), 104–117.
Tan, M.L., Ibrahim, A.L., Yusop, Z., Chua, V.P., Chan, N.W., 2017. Climate change impacts under CMIP5 RCP scenarios on water resources of the Kelantan River Basin. Malaysia. Atmos. Res. 189, 1–10.
Tan, X., Gan, T.Y., Chen, Y.D., 2018a. Moisture sources and pathways associated with the spatial variability of seasonal extreme precipitation over Canada. Clim. Dyn. 50 (1), 629–640.
Tan, X., Gan, T.Y., Chen, Y.D., 2018b. Synoptic moisture pathways associated with mean and extreme precipitation over Canada for summer and fall. Clim. Dyn. https://doi.org/10.1007/s00382-018-4300-6.
Taylor, G., Barrett, H., Funk, D., Nowlen, S., 2011. Advances in Understanding the Phenomena of Electrical Cable Fire-Induced Hot Shorting, Invited. pp. 485–486.
Thompson, J.R., Green, A.J., Kingston, D.G., Gosling, S.N., 2013. Assessment of uncertainty in river flow projections for the Mekong River using multiple GCMs and hydrological models. J. Hydrol. 486, 1–30.
Tong, K., Su, F., Yang, D., Hao, Z., 2014. Evaluation of satellite precipitation retrievals and their potential utilities in hydrologic modeling over the Tibetan Plateau. J. Hydrol. 519(A, 423–437.
Viviroli, D., Dürr, H.H., Messerli, B., Meybeck, M., Weingartner, R., 2007. Mountains of the world, water towers for humanity: Typology, mapping, and global significance. Water Resour. Res. 43 (7), 685–698.
Wang, L., Chen, W., 2013. A CMIP5 multimodel projection of future temperature, precipitation, and climatological drought in China. Int. J. Climatol. 34 (6), 2059–2078.
Wang, B., Bao, Q., Hoskins, B., Wu, G., Liu, Y., 2008. Tibetan Plateau warming and precipitation changes in East Asia. Geophys. Res. Lett. 35 (14), 63–72.
Wang, Z., Lai, C., Chen, X., Yang, B., Zhao, S., Bai, X., 2015. Flood hazard risk assessment model based on random forest. J. Hydrol. 527, 1130–1141.
Wang, Z., Zhang, H., Zhang, X., 2016. Projected response of East Asian summer monsoon system to future reductions in emissions of anthropogenic aerosols and their precursors. Clim. Dyn. 47 (5), 1455–1468.
Wang, W., Ding, Y., Shao, Q., Xu, J., Jiao, X., Luo, Y., Yu, Z., 2017a. Bayesian multi-model projection of irrigation requirement and water use efficiency in three typical rice plantation region of China based on CMIP5. Agric. For. Meteorol. 232, 89–105.
Wang, W., Lu, H., Ruby Leung, L., Li, H., Zhao, J., Tian, F., Yang, K., Sothea, K., 2017b. Dam construction in Lancang-Mekong River Basin could mitigate future flood risk from warming-induced intensified rainfall. Geophys. Res. Lett. 44 (20), 10,378–10,386.
Wang, Z., Zhong, R., Lai, C., Chen, J., 2017c. Evaluation of the GPM IMERG satellite-based precipitation products and the hydrological utility. Atmos. Res. 196, 151–163.
Wang, Z., Zhong, R., Lai, C., Zeng, Z., Lian, Y., Bai, X., 2017d. Climate change enhances the severity and variability of drought in the Pearl River Basin in South China in the 21st century. Agric. Forest Meteorol. 249 (2018), 149–162.
Wang, Z., Li, J., Lai, C., Wang, R.Y., Chen, X., Lian, Y., 2018. Drying tendency dominating the global grain production area. Global Food Secur. 16, 138–149.
Werner, A.T., Cannon, A.J., 2016. Hydrologic extremes - an intercomparison of multiple gridded statistical downscaling methods. Hydrol. Earth Syst. Sci. Discuss. 12 (6), 6179–6239.
Winsemius, H.C., Aerts, J.C.J.H., Beek, L.P.H.V., Bierkens, M.F.P., Bouwman, A., Jongman, B., Kwadijk, J.C.J., Ligtvoet, W., Lucas, P.L., Vuuren, D.P.V., 2015. Global drivers of future river flood risk. Nat. Clim. Chang. 6 (4).
Wu, H., Kimball, J.S., Mantua, N., Stanford, J., 2011. Automated upscaling of river networks for macroscale hydrological modeling. Water Resour. Res. 47 (3), 3517.
Wu, H., Kimball, J.S., Li, H., Huang, M., Leung, L.R., Adler, R.F., 2012. A new global river network database for macroscale hydrologic modeling. Water Resour. Res. 48 (9).
Wu, X., Wang, Z., Guo, S., Liao, W., Zeng, Z., Chen, X., 2017. Scenario-based projections of future urban inundation within a coupled hydrodynamic model framework: a case study in Dongguan City, China. J. Hydrol. 547, 428–442.
Wu, X., Guo, S., Yin, J., Yang, G., Zhong, Y., Liu, D., 2018. On the event-based extreme precipitation across China: Time distribution patterns, trends, and return levels. J. Hydrol. 562, 305–317.
Xie, Z., Yuan, F., Duan, Q., Zheng, J., Liang, M., Chen, F., 2007. Regional parameter estimation of the VIC land surface model: methodology and application to River Basins in China. J. Hydrometeorol. 8 (3), 447.
Yan, D., Werners, S.E., Ludwig, F., Huang, H.Q., 2015. Hydrological response to climate change: the Pearl River, China under different RCP scenarios. J. Hydrol. 4, 228–245.
Yang, K., Wu, H., Qin, J., Lin, C., Tang, W., Chen, Y., 2014. Recent climate changes over the Tibetan Plateau and their impacts on energy and water cycle: a review. Glob. Planet. Chang. 112, 79–91.
Yuan, F., Zhao, C., Jiang, Y., Ren, L., Shan, H., Zhang, L., Zhu, Y., Chen, T., Jiang, S., Yang, X., Shen, H., 2017. Evaluation on uncertainty sources in projecting hydrological changes over the Xijiang River basin in South China. J. Hydrol. 554, 434–450.
Zhang, Y., Su, F., Hao, Z., Xu, C., Yu, Z., Wang, L., Tong, K., 2015. Impact of projected climate change on the hydrology in the headwaters of the Yellow River basin. Hydrol. Process. 29, 4379–4397. https://doi.org/10.1002/hyp.10497.
Zhang, L., Su, F., Yang, D., Hao, Z., Tong, K., 2013. Discharge regime and simulation for the upstream of major rivers over Tibetan Plateau. J. Geophys. Res. Atmos. 118 (15), 8500–8518.
Zhang, Y., You, Q., Chen, C., Ge, J., 2016. Impacts of climate change on streamflows under RCP scenarios: a case study in Xin River Basin, China. Atmos. Res. 178-179, 521–534.
Zhao, Q., Liu, S., Deng, L., Dong, S., Cong, Wang, Yang, Z., Yang, J., 2012. Landscape change and hydrologic alteration associated with dam construction. Int. J. Appl. Earth Obs. Geoinf. 16 (1), 17–26.